Greaves, SJ., Rose, RA., Abou-Chahine, F., Glowacki, DR., Troya, D., & Orr-Ewing, AJ. (2011). Quasi-classical trajectory study of the dynamics of the Cl + CH4→ HCl + CH3 reaction. *Physical Chemistry Chemical Physics*, *13*, 11438 - 11445. https://doi.org/10.1039/C0CP02694H

Quasi-classical trajectory study of the dynamics of the Cl + CH_4 → HCl + CH_3 reaction

S.J. Greaves,[1,*] R.A. Rose,[1] F. Abou-Chahine,[1] D.R. Glowacki,[1] D. Troya[2] and A.J. Orr-Ewing[1]

[1] School of Chemistry, University of Bristol, Cantock's Close, Bristol BS8 1TS, UK.

[2] Department of Chemistry, Virginia Tech, 107 Davidson Hall, Blacksburg, Virginia 24061-0212, USA.

12 August 2014

* Author for correspondence

Tel: 0117 9289938

Fax: 0117 9250612

e-mail: s.j.greaves@bris.ac.uk

Figures: 5

Tables: 3

Abstract

We present an on-the-fly classical trajectory study of the Cl + $CH_4 \rightarrow$ HCl + CH_3 reaction using a specific reaction parameter (SRP) AM1 Hamiltonian that was previously optimized for the Cl + ethane reaction [S. J. Greaves *et al.*, *J. Phys Chem A*, 2008, **112**, 9387]. The SRP-AM1 Hamiltonian is shown to be a good model for the potential energy surface of the title reaction. Calculated differential cross sections, obtained from trajectories propagated with the SRP-AM1 Hamiltonian compare favourably with experimental results for this system. Analysis of the vibrational modes of the methyl radical shows different scattering distributions for ground and vibrationally excited products.

I. Introduction

The abstraction of an H atom from CH_4 by a Cl atom, and the reverse reaction of CH_3 radicals with HCl, are now firmly established as benchmark systems for study of the dynamics of chemical reactions of polyatomic molecules.[1] Over more than a decade, experiments have examined phenomena exhibited by these reactions such as quantum-state specific angular scattering,[2, 3] mode and bond-specific chemistry,[2, 4-9] dynamical stereochemistry,[5] non-adiabaticity,[10-13] and scattering resonances.[14] Theoretical investigations stimulated by the wealth of experimental data have included generation of semi-empirical[15-18] and *ab initio*[18-20] potential energy surfaces (PESs) and computation of reactive scattering by quasi-classical trajectory (QCT)[15, 16, 21] or quantum mechanical (QM) scattering methods.[18, 22-25] Very recently, QM scattering calculations have been performed that incorporate non-adiabatic dynamics on three coupled PESs.[26] In many of the computational studies, the number of degrees of freedom is reduced from the full dimensionality of the 6-atom $Cl + CH_4 \rightarrow HCl + CH_3$ reaction. PESs that encompass all the degrees of freedom have, however, been reported, including hypersurfaces derived from fits to *ab initio* points of LEPS (London-Eyring-Polanyi-Sato) functions augmented by bending potential terms.[15, 18, 27] A first accurate, fully dimensional *ab initio* PES was generated by Castillo *et al*.[20] using the iterative interpolation method of Collins and co-workers,[28-31] and was subsequently employed for QCT calculations. In this latter study, QCISD electronic structure calculations were carried out with an aug-cc-pVDZ basis set, and the scaling all correlations method[32, 33] was used to correct inaccuracies of the applied level of theory to reduce the computed barrier height.

To avoid computation of a global PES for studies of the mechanisms of reactions of polyatomic molecules such as methane, an alternative approach is to propagate direct dynamics trajectories with on-the-fly computation of potential energies and gradients. This strategy has already proved successful for the $Cl + CH_4$ reaction, with Troya and Weiss demonstrating the use of re-parameterized semi-empirical Hamiltonians to study the scattering dynamics with incorporation of all degrees of freedom.[16] The optimization of the parameters of a semi-empirical Hamiltonian, typically by fitting to energies computed by high-level electronic structure calculations at selected molecular geometries, has been employed for the study of a number of chemical reactions.[16, 34-37] This specific reaction parameter (SRP) approach enables trajectories to be propagated in direct dynamics calculations with lower computational demand at each step of the trajectory than would be required for energy calculations using methods based on *ab initio* computation (e.g. Hartree-Fock approaches) or density functional theory (DFT). Propagation of batches of trajectories in sufficient

numbers for statistical sampling of the initial conditions and averaging of final outcomes therefore becomes tractable for reactions as complicated as that of Cl atoms with CH_4, without the need to impose constraints such as initiation of reactions at the transition state (TS) geometry.[38]

Here, we examine how successfully an SRP Hamiltonian optimized for one particular reaction can be applied to the study of another related but distinct chemical reaction. In so doing, we evaluate a possible strategy to by-pass calculation of specific global PESs for every individual reaction. We previously reported use of an SRP-AM1 Hamiltonian for the study of the reaction Cl + $C_2H_6 \rightarrow$ HCl + C_2H_5 in which the reaction parameters were fitted to *ab initio* energies computed at the CCSD(T)/aug-cc-pVDZ level for numerous geometries, most of which were selected to cover the region of the PES in proximity to the intrinsic reaction coordinate (IRC).[35, 36] This mildly exothermic (by -8.8$\pm$1.7 kJ mol^{-1}) reaction is characterized by a low barrier (an activation energy of 0.62$\pm$0.01 kJ mol^{-1} is derived from analysis of thermal rate constants at temperatures in the range 177 – 353 K) that is late on the reaction coordinate. In contrast, the Cl + CH_4 reaction that is the subject of the current study has a late barrier of ~11.3 kJ mol^{-1} (and thus a thermal rate constant that is ~600 times smaller at 298 K than for the Cl + C_2H_6 reaction), and the reaction is endothermic by +7.6$\pm$0.4 kJ mol^{-1}. Despite these differences, we demonstrate that the use of an SRP-AM1 Hamiltonian optimized for reaction of Cl atoms with ethane can also be successfully employed for QCT calculations that describe well the dynamics of the Cl + CH_4 reaction. We compare the performance of the SRP-AM1 Hamiltonian with the previously employed re-parameterizations of AM1, PM3 and MSINDO Hamiltonians by Troya and Weiss for this same reaction.[16]

II. Theoretical and Computational Methods

The method employed to fit the parameters of the AM1 Hamiltonian for our prior investigation of the Cl + C_2H_6 reaction (and here employed for the Cl + CH_4 reaction without further modification) has been described in detail elsewhere,[35, 36] and only a brief review is presented here. The stationary points of the Cl + C_2H_6 reaction (reagents, pre-TS complex, TS, post-TS complex and products) were characterized using MP2/aug-cc-pVDZ optimized geometries and CCSD(T) energies extrapolated to the complete basis limit, giving results within 4 kJ mol^{-1} of experimental values. The IRC was mapped by scanning the Cl—HCH_2CH_3 distance on the approach to the TS and the ClH—CH_2CH_3 distance following passage through the TS, with geometries optimized at the MP2/aug-cc-pVDZ level and energies calculated with the CCSD(T)/aug-cc-pVDZ method. Values of the specific reaction

parameters of the AM1 Hamiltonian were then obtained in a fitting procedure which minimized the energy difference between the *ab initio* and the equivalent SRP-AM1 points.[35, 36]

The suitability of using the SRP-AM1 Hamiltonian developed for the Cl + ethane reaction to model the Cl + $CH_4 \rightarrow$ HCl + CH_3 reaction can be assessed by comparing the energetics for the latter reaction, calculated with the SRP-AM1 Hamiltonian, to outcomes for previously derived SRP Hamiltonians and high level *ab initio* calculations, as well as experimental data, as shown in **Table I**. The SRP-AM1 reaction energy is within ~2.5 kJ mol^{-1} of the experimental value, an improvement upon the previous SRP-MSINDO[16] and QCISD-SAC/aug-cc-pvdz[20] methods. The barrier height is within 0.7 kJ mol^{-1} of best high level calculations and the activation energy from Arrhenius analysis of the temperature dependence of the rate coefficients.[39] The computed geometry of the SRP-AM1 TS, shown in **Table II**, has bond lengths within 0.02 Å, and angles within 1.1° of CCSD(T) and QCISD-SAC calculations. **Table III** shows a comparison of calculated and experimental harmonic normal mode frequencies. The superior performance of the SRP-AM1 Hamiltonian over the SRP-MSINDO method[16] in the calculation of vibrational frequencies (when compared to both experiment and higher level CCSD(T)/aug-ccpVTZ calculations) is evident, with over-estimation of harmonic frequencies by the MSINDO method by ~20%. The change in zero-point energy (ΔZPE) for the reaction at the SRP-AM1 level is just 17 cm^{-1} higher than the equivalent CCSD(T) calculation and only 147 cm^{-1} from the experimental value. The improved performance of the SRP-AM1 method for the Cl + CH_4 reaction may derive from its parameter optimization for the Cl + C_2H_6 reaction, which used IRC scans with the C-H-Cl bond angle fixed at 180° (despite the extra methyl group in ethane stabilising the TS at a slightly bent geometry). This same angle defines the C_{3v} symmetry of the TS and IRC C-H-Cl bond angle in the title reaction.

The outcomes of IRC scans along the collinear Cl + CH_4 reaction path using the SRP-AM1 Hamiltonian are shown in **Figure 1**, and are compared with results from higher level *ab initio* calculations and the SRP-MSINDO Hamiltonian. As is the case for the Cl + ethane reaction,[35, 36] the SRP-AM1 Hamiltonian shows good agreement with the *ab initio* calculations, effectively modelling the energies of the products and TS relative to the reagents. Panels (c) and (d) of **Figure 1** display the PES as the C-H-Cl angle is bent away from the C_{3v} geometry of the minimum energy path. The post-TS minimum, caused by dipole-quadrupole interactions, is also well reproduced by the SRP-AM1 Hamiltonian. Despite the relatively shallow depth (13.24 kJ mol^{-1} below the TS and 7.95 kJ mol^{-1} below the products), this minimum may be significant in the reaction dynamics as the excess collision energy over the barrier employed in the calculations here is only ~4 kJ mol^{-1}. The post-TS interactions between separating CH_3 and HCl products induced by this shallow well may have an influence on the

rotational motion of the HCl products,[1, 40] arresting rotational excitation because of the associated collinear Cl-H-C geometry.

III. Trajectory Calculations

IIIA: Initial Conditions Sampling

Sampling of initial conditions was carried out using a version of the VENUS dynamics package[41, 42] modified to interface with arbitrary electronic structure theory packages. For this work, VENUS was interfaced with a modified version of GAMESS-US[43] in which energy and gradient evaluations are available using the SRP-AM1 Hamiltonian. Initial coordinates and momenta for methane having zero-point motion were selected using a classical random phase approximation and microcanonical normal mode sampling,[44] in which all methane normal mode quantum numbers were set to $v = 0$. The relative translational energy between the Cl and CH_4 fragments was chosen to be 15.4 kJ mol^{-1}, to be comparable with previous experimental[45] and theoretical[16] studies of this reaction. The rotational energy of CH_4 was set to zero, and its initial orientation was determined by random rotation in the molecular centre-of-mass (COM) Eckart frame. Trajectories were initialized with a 5.5 Å COM separation between the CH_4 and Cl fragments and an impact parameter, *b*, randomly chosen between 0 and 3 Å, beyond which the reaction probability was negligible (as is discussed below). The initial coordinates and momenta generated using the VENUS-GAMESS-US interface were then passed to the GAMESS-US program, with which energy gradients along all coordinates at each time step were calculated on-the-fly employing the SRP-AM1 Hamiltonian within the dynamic-reaction-coordinate (DRC) function.[46] Integration of the classical equations of motion was undertaken with a time step of 0.05 fs until the termination criterion, a C atom – Cl atom separation of 7Å, was reached. This integration typically required 8000-12000 time steps. The DRC function ensures total energy conservation for each trajectory to better than 0.13 kJ mol^{-1}.

IIIB: Analysis of trajectories

Trajectories were analyzed using atomic coordinates and momenta provided by the DRC function, from which experimentally comparable observables could be determined. Analysis of product scattering angles (the scattering angle, θ, is defined as that between the velocity vectors of reagent Cl and product HCl in the COM frame), the translational energy of the products, and the internal energy of HCl were carried out as reported in our previous paper.[36] Our analysis of the internal

energy of the radical product (CH_3), however, incorporates additional calculation of the energy disposal into the normal modes of CH_3. For the reactive trajectories, energy disposal in the nascent CH_3 was determined by projecting its space-fixed cartesian velocities, $\dot{\mathbf{q}}(t)$, and coordinates, $\mathbf{q}(t)$, onto the 3*N* translational, rotational, and vibrational degrees of freedom of CH_3 in its SRP-AM1 COM frame equilibrium geometry, $\mathbf{q}_{eq}(t)$. In order to carry out this analysis, the nascent CH_3 was translated to its COM frame, and the least squares difference between the mass weighted coordinates of the nascent CH_3 and that of equilibrium CH_3 was minimized using singular value decomposition. This operation places the rovibrationally hot CH_3 into the Eckart frame of the equilibrium CH_3, thereby minimizing rovibrational Coriolis coupling in the nascent CH_3.[47-50] The projection of the Cartesian coordinates and velocities into the translational, rotational, and vibrational displacements of the equilibrium geometry was then accomplished via the following relationships:[51]

$$\Delta\mathbf{Q}(t) = \mathbf{L}^{-1}\Delta\mathbf{q}(t)$$
$$\dot{\mathbf{Q}}(t) = \mathbf{L}^{-1}\dot{\mathbf{q}}(t)$$

where $\Delta\mathbf{q}(t) = \mathbf{q}(t) - \mathbf{q}_{eq}(t)$ is the vector of cartesian displacements from equilibrium for a particular CH_3 geometry. $\Delta\mathbf{Q}(t)$ and $\dot{\mathbf{Q}}(t)$ are the respective velocity and coordinates vectors of the nascent CH_3 in the normal mode frame, and $\mathbf{L}$ is a 3N × 3N matrix composed of normalized cartestian displacement vectors corresponding to the 3 translational, 3 rotational, and 3N-6 vibrational coordinates. The translational and rotational eigenvectors were obtained from first principles in the usual way,[52] and the vibrational eigenvectors were determined from diagonalization of the optimized CH_3 Hessian. The frequencies of equilibrium CH_3 are given in **Table III**. Similar methodologies for calculating the internal energy disposal of a polyatomic product of a classical trajectory have been recently described, see for example Ref. 53 and 54.

Total vibrational mode energies in the nascent CH_3 were obtained by using a harmonic approximation to determine the potential energy in each mode from $\Delta\mathbf{Q}(t)$, and adding it to the kinetic energy in each mode, determined from $\dot{\mathbf{Q}}(t)$. The reported energies were obtained by averaging over the final 3000 steps of each reactive trajectory. Classical quantization of vibrational and rotational motion was achieved by dividing by the energy of a vibrational quantum of the respective mode, and rounding to the nearest integer value.

IV. Results and discussion

Of the 45,000 trajectories calculated, 2930 were reactive, corresponding to a success rate of only ~6% as a consequence of the low collision energy. Classical mechanics does not rigorously conserve ZPE, so that products may be formed with internal energies below the nominal zero-point level. After applying a passive ZPE leakage correction to accept radical products with internal energies that lie above a threshold chosen to be 5.4 kJ mol^{-1} below the ZPE level (an amount that we consider to be of acceptable chemical accuracy), only 751 successful reactive trajectories remained. Previous QCT calculations of the reaction of Cl atoms with methane[15] and with ethane[35, 36] showed evidence for a chattering mechanism in which the light H atom moves repeatedly between the C and Cl atoms before forming products. All reactive trajectories were analysed for signatures of chattering[35] and a total of 154 trajectories showed this behaviour, 59 of which satisfied the above-mentioned criterion for sufficient ZPE in the products.

The calculated differential cross section (DCS) for the title reaction at a collision energy of 15.3 kJ mol^{-1} is shown in **Figure 2** where trajectories leading to ground-state methyl products, $CH_3(v=0)$, and umbrella-excited methyl, $CH_3(\nu_2 > 0)$, are compared to the experimental data of Liu and co-workers for the $Cl + CH_4 \rightarrow CH_3(v=0) + HCl$ reaction at a slightly higher mean collision energy of 17.2 kJ mol^{-1}.[55] The shapes of the calculated $CH_3(v=0)$, and experimental DCSs are qualitatively similar, with both demonstrating scattering predominantly in the backward and sideways directions. However, the calculated DCS shows a slightly greater propensity for forward scattering, with a peak at ~80˚, in contrast with the experiments, for which the DCS peaks at ~100˚ and cuts off between 90 and 60°.[55] Similar scattering behaviour was observed in previous calculations for the title reaction using the SRP-MSINDO Hamiltonian, and our DCS is in very good agreement with the one computed in that study.[16] The rise in scattering probability at low scattering angles was also observed in trajectories calculated on the QCISD-SAC PES,[20] however these trajectories did not show the reduction in scattering probability in the backwards scattering region that is observed in both the experimental and our SRP-AM1 calculations. A simple line-of-centres model[56] predicts a cut-off in the DCS for angles below 125° at the current collision energy, which is greater than observed both experimentally and in the QCT calculations. The greater forward scattering observed in the QCT calculations cannot be attributed to the barrier height on the PES because the value for the SRP-AM1 Hamiltonian is within 0.7 kJ mol^{-1} of the best *ab initio* calculations, and the experimentally derived activation energy value (**Table I**). There is very little difference between the DCSs produced by analysing all reactive trajectories and by restricting analysis to those that meet criteria for product ZPE. The violation of ZPE conservation has most significance for the more backwards scattered trajectories.

Analysis of total kinetic energy release (TKER) demonstrates that energy lost from the internal modes of trajectories which violate ZPE conservation is channelled into product translation. Comparing TKER distributions for trajectories that satisfy the ZPE criterion we observe the following: sideways and backward scattering regions (here we choose sideways to indicate the angular range θ=60-120˚, and backward to encompass θ=120-180˚) exhibit nearly identical TKER distributions, whereas the forward scattering region (here taken to be θ=0-60˚) shows distinctly less translational energy release in the products. The disparity in TKER between the forwards and sideways-backward regions results from the excitation of at least 1 quantum of the methyl product umbrella stretching mode ($CH_3(\nu_2)$); indeed, trajectories that exhibit scattering angles below 60° have a greater proportion with $\nu_2 > 0$ when compared with other scattering ranges.

The DCS shown in **Figure 2** for the trajectories that result in umbrella mode excitation is broader than that for ground state products and shows a small shift away from backward scattering towards the forwards direction. There has been no experimental measurement of the DCS for umbrella mode excited CH_3 products, however our calculations do behave in a similar manner to DCSs reported for an experimental study of the related reaction $O(^3P) + CD_4 \rightarrow OD + CD_3(\nu_2>0)$.[57]

Figure 2 also shows a plot demonstrating the strong correlation between scattering angle and impact parameter, *b*, with large *b* resulting in forward scattering and low values of *b* giving backward scattering. The correlation between *b* and θ is qualitatively similar to that found in the Cl + ethane reaction studied with the SRP-AM1 Hamiltonian (absolute values differ because of the larger maximum impact parameter required in the ethane case). A simple hard-sphere model for a reaction[56] predicts that cos θ is proportional to b^2,reproduces well the *b*-θ relationship observed in our study, as shown by the green line in panel (b) of **Figure 2**. The chattering trajectories are generally more forward scattered, but still cover the full range of scattering angles, in contrast to the results of Levine and co-workers[15] who predicted that the osculating, chattering trajectories would originate exclusively from high impact parameter collisions that lead to forward scattering. While the chattering trajectories do demonstrate greater forward scattering, the limited number of successful trajectories makes it difficult to identify a clear signature of chattering that might be probed experimentally.

The opacity function, shown in **Figure 3**, exhibits an even probability of reaction up to $b \approx 1.875$ Å where it decreases to a cut off at $b_{max} \approx 2.75$ Å. This limit to the distribution can easily be understood in terms of the TS structure which has a C-Cl distance of 2.85 Å. The opacity function shows the same sharp cut off at high impact parameter as was found in previous studies that employed the SRP-MSINDO methodology[16] and QCISD-SAC PES.[20]

The QCT-calculated rotational level population distribution of HCl products shown in **Figure 4** is hotter than experimentally determined, as has been noted previously, perhaps indicating exaggerated coupling between bending of the Cl-CH_4 TS and rotational motion of HCl.[16, 38] The HCl rotational distributions computed by classical trajectories for this reaction are insensitive to the PES used; the distribution shown in **Figure 4** is virtually identical to those obtained with the SRP-MSINDO PES[16] and with the high quality ab initio PES of Ref. 20, suggesting that QCT calculations are missing an important dynamical feature that quenches the HCl rotational motion. The exclusion of trajectories that violate ZPE conservation in the products improves the agreement of the J_{HCl} population distribution with experiment, reducing the range of J_{HCl} values and shifting the peak of the distribution down to J_{HCl}=3, but this remains higher than the experimental peak of J_{HCl}=1. The vibrational energy distribution of the methyl products is shown in **Figure 5**; the four panels show the excitation of the four vibrational modes of the methyl, calculated as described in section **IIIB**. These modes, denoted as ν_1- ν_4, correspond to the symmetric stretch, the umbrella bend, the asymmetric stretch and the scissor bend, respectively and their frequencies are listed in **Table III**. For trajectories that satisfy the ZPE criterion both the symmetric and asymmetric stretches show no vibrational excitation (as is expected on energy conservation grounds), in contrast to the lower frequency bending modes: the scissor bend shows some modest excitation to v_4=1, while the umbrella mode is excited in 29% of trajectories, with up to 3 quanta being populated. The vibrational excitation of the chattering trajectories displays the same distribution as the non-chattering trajectories, showing no sign of the enhanced internal energies suggested previously.[58] Some degree of the excitation of the umbrella mode is expected from geometric arguments, because prompt abstraction of an H atom from methane would leave the CH_3 group in the tetrahedral geometry displaced along the umbrella mode from its D_{3h} equilibrium structure. As was noted earlier the DCS for umbrella mode excited trajectories is shifted slightly towards the forwards region compared with ground state products.

V. Conclusions

Quasiclassical trajectories have been calculated on-the-fly for the Cl + $CH_4 \rightarrow CH_3$ + HCl reaction using a SRP-AM1 Hamiltonian to describe the PES that was previously optimized for a trajectory study of the related Cl + ethane reaction. The successful application of the specific reaction parameters developed for one reaction to a related, but in some respects significantly different, reaction encourages the possibility of using optimized SRPs for efficient calculation of trajectories for a family of reactions with similar features. Outcomes of our QCT calculations compare favourably

with previous classical trajectory calculations on the Cl + CH_4 reaction. There is broad agreement between the experimental and theoretical DCSs, though with greater forward scatter in the calculated differential cross section than is reported from crossed beam experiments. Normal mode energy analysis of the methyl radical product reveals no excitation in the stretching modes, but excitation of up to 3 quanta of the umbrella bend is observed, and trajectories with this excitation are more prevalent in the forwards scattering direction. The HCl rotational distribution is however hotter than that measured experimentally.

Acknowledgements

The Bristol group thanks EPSRC for funding via the Programme Grant EP/G00224X. AJOE gratefully acknowledges the Royal Society and Wolfson Foundation for a Research Merit Award, and SJG thanks the Leverhulme Trust for the award of an Early Career Fellowship. DT thanks the NSF for support through Grant No. CHE-0547543.

References

1. C. Murray and A. J. Orr-Ewing, *Int. Rev. Phys. Chem.*, 2004, **23**, 435
2. W. R. Simpson, A. J. Orr-Ewing and R. N. Zare, *Chem. Phys. Lett.*, 1993, **212**, 163.
3. M. J. Bass, M. Brouard, R. Cireasa, A. P. Clark and C. Vallance, *J. Chem. Phys.*, 2005, **123**, 094301.
4. Z. H. Kim, H. A. Bechtel, J. P. Camden and R. N. Zare, *J. Chem. Phys.*, 2005, **122**, 084303.
5. A. J. Orr-Ewing, W. R. Simpson, T. P. Rakitzis, S. A. Kandel and R. N. Zare, *J. Chem. Phys.*, 1997, **106**, 5961.
6. S. Yoon, S. Henton, A. N. Zirkovic and F. F. Crim, *J. Chem. Phys.*, 2002, **116**, 10744.
7. S. Yoon, R. J. Holiday, I. E. L. Silbert and F. F. Crim, *J. Chem. Phys.*, 2003, **119**, 9568.
8. R. J. Holiday, C. H. Kwon, C. J. Annesley and F. F. Crim, *J. Chem. Phys.*, 2006, **125**, 133101.
9. S. Yan, Y.-T. Wu, B. Zhang, X.-F. Yue and K. Liu, *Science*, 2007, **316**, 1723.
10. J. Zhou, J. J. Lin, B. Zhang and K. Liu, *J. Phys. Chem. A*, 2004, **108**, 7832.
11. B. Retail, S. J. Greaves, J. K. Pearce, R. A. Rose and A. J. Orr-Ewing, *Phys. Chem. Chem. Phys.*, 2007, **9**, 3261.
12. B. Retail, J. K. Pearce, S. J. Greaves, R. A. Rose and A. J. Orr-Ewing, *J. Chem. Phys.*, 2008, **128**, 184303.
13. B. Retail, J. K. Pearce, C. Murray and A. J. Orr-Ewing, *J. Chem. Phys.*, 2005, **122**, 101101.
14. B. Zhang and K. Liu, *J. Chem. Phys.*, 2005, **122**, 101102.
15. X. Wang, M. Ben-Nun and R. D. Levine, *Chem. Phys.*, 1995, **197**, 1.
16. D. Troya and P. J. E. Weiss, *J. Chem. Phys.*, 2006, **124**, 074313.
17. C. Rangel, M. Navarrete, J. C. Corchado and J. Espinosa-García, *J. Chem. Phys.*, 2006, **124**, 124306.
18. M.-y. Yang, C.-L. Yang, J.-z. Chen and Q.-g. Zhang, *Chem. Phys.*, 2008, **354**, 180.
19. J. C. Corchado, D. G. Truhlar and J. Espinosa-Garcia, *J. Chem. Phys.*, 2000, **112**, 9375.

20. J. F. Castillo, F. J. Aoiz and L. Banares, *J. Chem. Phys.*, 2006, **125**, 124316.
21. J. Espinosa-García, *J. Phys. Chem. A*, 2007, **111**, 5792.
22. H.-G. Yu and G. Nyman, *J. Chem. Phys.*, 1999, **110**, 7233.
23. H.-G. Yu and G. Nyman, *J. Chem. Phys.*, 1999, **111**, 6693.
24. S. T. Banks and D. C. Clary, *Phys. Chem. Chem. Phys.*, 2007, **9**, 933.
25. R. Martinez, M. Gonzalez, P. Defazio and C. Petrongolo, *J. Chem. Phys.*, 2007, **127**, 104302.
26. S. Remmert and D. Clary, private communication, 2010.
27. J. Espinosa-García, *J. Phys. Chem. A*, 2007, **111**, 9654.
28. R. P. A. Bettens and M. A. Collins, *J. Chem. Phys.*, 1999, **111**, 816.
29. M. A. Collins, *Theoretical Chemistry Accounts: Theory, Computation, and Modeling (Theoretica Chimica Acta)*, 2002, **108**, 313.
30. M. J. T. Jordan, K. C. Thompson, M. A. Collins and R. P. A. Bettens, *J. Chem. Phys.*, 1995, **102**, 5647.
31. K. C. Thompson, M. J. T. Jordan and M. A. Collins, *J. Chem. Phys.*, 1998, **108**, 8302.
32. M. S. Gordon and D. G. Truhlar, *J. Am. Chem. Soc.*, 1986, **108**, 5412.
33. P. L. Fast, J. Corchado, M. L. Sanchez and D. G. Truhlar, *J. Phys. Chem. A*, 1999, **103**, 3139.
34. A. Gonzalez-Lafont, T. N. Truong and D. G. Truhlar, *J. Phys. Chem.*, 1991, **95**, 4618.
35. S. J. Greaves, J. Kim, A. J. Orr-Ewing and D. Troya, *Chem. Phys. Lett.*, 2007, **441**, 171.
36. S. J. Greaves, A. J. Orr-Ewing and D. Troya, *J. Phys. Chem. A*, 2008, **112**, 9387.
37. A. Fernández-Ramos, E. Martínez-Núñez, J. M. C. Marques and S. A. Vázquez, *J. Chem. Phys.*, 2003, **118**, 6280.
38. S. Rudić, C. Murray, J. N. Harvey and A. J. Orr-Ewing, *J. Chem. Phys.*, 2004, **120**, 186.
39. M. S. Zahniser, B. M. Berquist and F. Kaufman, *Int. J. Chem. Kinet.*, 1978, **10**, 15.
40. C. Murray, J. K. Pearce, S. Rudić, B. Retail and A. J. Orr-Ewing, *J. Phys. Chem. A*, 2005, **109**, 11093.
41. X. C. Hu, W. L. Hase and T. Pirraglia, *J. Comput. Chem.*, 1991, **12**, 1014.
42. W. L. Hase, R. J. Duchovic, X. Hu, A. Komornicki, K. F. Lim, D.-h. Lu, G. H. Peslherbe, K. N. Swamy, S. R. V. Linde, A. Varandas, H.Wang and R. J. Wolf, *QCPE Bull.*, 1996, **16**, 671.
43. M. W. Schmidt, K. K. Baldridge, J. A. Boatz, S. T. Elbert, M. S. Gordon, J. H. Jensen, S. Koseki, N. Matsunaga, K. A. Nguyen, S. J. Su, T. L. Windus, M. Dupuis and J. A. Montgomery, *J. Comput. Chem.*, 1993, **14**, 1347.
44. W. L. Hase and D. G. Buckowski, *Chem. Phys. Lett.*, 1980, **74**, 284.
45. C. Murray, B. Retail and A. J. Orr-Ewing, *Chem. Phys.*, 2004, **301**, 239.
46. M. W. Schmidt, M. S. Gordon and M. Dupuis, *J. Am. Chem. Soc.*, 1985, **107**, 2585.
47. J. H. Challis, *J. Biomech.*, 1995, **28**, 733.
48. E. A. Coutsias, C. Seok and K. A. Dill, *J. Comput. Chem.*, 2005, **26**, 1663.
49. G. R. Kneller, *J. Chem. Phys.*, 2008, **128**, 6.
50. K. N. Kudin and A. Y. Dymarsky, *J. Chem. Phys.*, 2005, **122**, 2.
51. L. M. Raff, *J. Chem. Phys.*, 1988, **89**, 5680.
52. W. H. Miller, N. C. Handy and J. E. Adams, *J. Chem. Phys.*, 1980, **72**, 99.
53. G. Czako and J. M. Bowman, *J. Chem. Phys.*, 2009, **131**, 244302.
54. J. C. Corchado and J. Espinosa-Garcia, *Phys. Chem. Chem. Phys.*, 2009, **11**, 10157.
55. J. Zhou, J. J. Zhang and K. Liu, *Mol. Phys.*, 2005, **103**, 1757.
56. W. R. Simpson, T. P. Rakitzis, S. A. Kandel, T. Lev-On and R. N. Zare, *J. Phys. Chem.*, 1996, **100**, 7938.
57. B. Zhang and K. Liu, *J. Phys. Chem. A*, 2005, **109**, 6791.
58. C. Huang, W. Li and A. G. Suits, *J. Chem. Phys.*, 2006, **125**, 133107.
59. A. Halkier, T. Helgaker, P. Jorgensen, W. Klopper, H. Koch, J. Olsen and A. K. Wilson, *Chem. Phys. Lett.*, 1998, **286**, 243.
60. , NIST Computational Chemistry Comparison and Benchmark Database,
NIST Standard Reference Database Number 101

Release 15a, April 2010, Editor: Russell D. Johnson III
http://cccbdb.nist.gov/ edn.

Tables

Table I. Computed barrier heights and reaction energies for the Cl + $CH_4 \rightarrow HCl + CH_3$ reaction. Values in parentheses correspond to classical energies, i.e., without including zero-point energy.

	Barrier / kJ mol^{-1}	Reaction energy / kJ mol^{-1}
CCSD(T)/aug-cc-pvdz [a]	16.40 (34.02)	7.95 (28.95)
CCSD(T)/aug-cc-pvtz [a]	15.23 (32.72)	5.19 (26.90)
CCSD(T)/aug-cc-pvqz // CCSD(T)/aug-cc-pvtz [a]	12.80 (30.29)	1.80 (23.51)
CCSD(T)/CBL[b] // CCSD(T)/aug-cc-pvtz [a]	11.05 (28.53)	-0.67 (21.05)
CCSD(T)/cc-pvtz [a]	22.68 (40.38)	9.25 (30.75)
CCSD/aug-cc-pvdz [a]	23.64 (41.05)	9.00 (30.17)
CCSD(T)/aug-cc-pvdz // CCSD/aug-cc-pvdz [a]	16.40 (34.02)	7.95 (28.95)
QCISD-SAC/aug-cc-pvdz[20]	15.86 (32.97)	7.57 (27.95)
SRP-MSINDO/ROHF [a]	14.14 (34.64)	-0.71 (25.23)
CTE[19] PES	12.97 (32.22)	3.77 (25.52)
SRP-AM1	**11.55 (31.76)**	**6.90 (28.58)**
Experiment [c]	10.88±1.67[d]	4.60±0.42 (23.85±0.42)

[a] CCSD(T) and SRP-MSINDO values are taken from Ref. 16.

[b] Complete basis set limit estimated according to a two-point extrapolation procedure[59] employing single point energies at the CCSD(T)/aug-cc-pvqz and CCSD(T)/aug-cc-pvtz levels.

[c] Enthalpy of reaction at 0 K obtained from the experimental heats of formation of Ref. 60 The classical value of the experimental reaction energy has been calculated using the experimental reaction energy and the experimental fundamental normal-mode frequencies taken from Ref. 60

[d] Activation energy estimated from the Arrhenius representation of the thermal rate constants from Ref. 39.

Table II. Calculated geometrical parameters of the C_{3v} symmetry saddle point of the Cl + CH_4 $\rightarrow$ HCl + CH_3 reaction.[a]

	R(H-Cl) / Å	R(H-C) / Å	R(H'-C) / Å	H'-C-H /°
CCSD(T)/aug-cc-pvdz	1.451	1.418	1.097	100.8
CCSD(T)/aug-cc-pvtz	1.445	1.404	1.088	101.0
CCSD(T)/cc-pvtz	1.442	1.406	1.084	101.0
CCSD/aug-cc-pvdz	1.460	1.401	1.096	101.1
QCISD-SAC/aug-cc-pvdz[20]	1.441	1.423	1.098	101.1
SRP-MSINDO /ROHF	1.449	1.318	1.106	103.6
CTE-PES	1.356	1.389	1.098	107.4
SRP-AM1	**1.446**	**1.406**	**1.097**	**99.9**

[a] H denotes the hydrogen undergoing abstraction and H′ is a non-abstracted C_{3v} symmetry-equivalent hydrogen atom.

Table III. Calculated harmonic normal-mode frequencies (cm^{-1}) of reagents, products, and the saddle point of the $Cl+CH_4 \rightarrow HCl+CH_3$ reaction. All the semiempirical calculations employed a ROHF reference.

	SRP-AM1	SRP-MSINDO	CCSD(T)/aug-cc-pvtz[a]	Experimental
CH_4				
	3130	3909	3147 (T_2)	3019
	3259	3737	3028 (A_1)	2917
	1437	1638	1573 (E)	1534
	1420	1679	1350 (T_2)	1306
CH_3				
ν_1	3278	3802	3114 (A_1')	3004
ν_2	958	905	496 (A_2")	606
ν_3	3300	4011	3295 (E')	3161
ν_4	1383	1566	1419 (E')	1396
HCl				
	2562	3542	2992 (Σ^+)	2991
TS				
	3185	3892	3238 (E)	
	3216	3737	3069 (A_1)	
	1371	1568	1407 (E)	
	1400	1594	1176 (A_1)	
	875	1196	886 (E)	
	514	685	520 (A_1)	
	210	502	350 (E)	
	1017i	1262i	973i (A_1)	

[a]The symmetries of the normal modes are shown in the CCSD(T)/aug-cc-pvtz column.

Figures

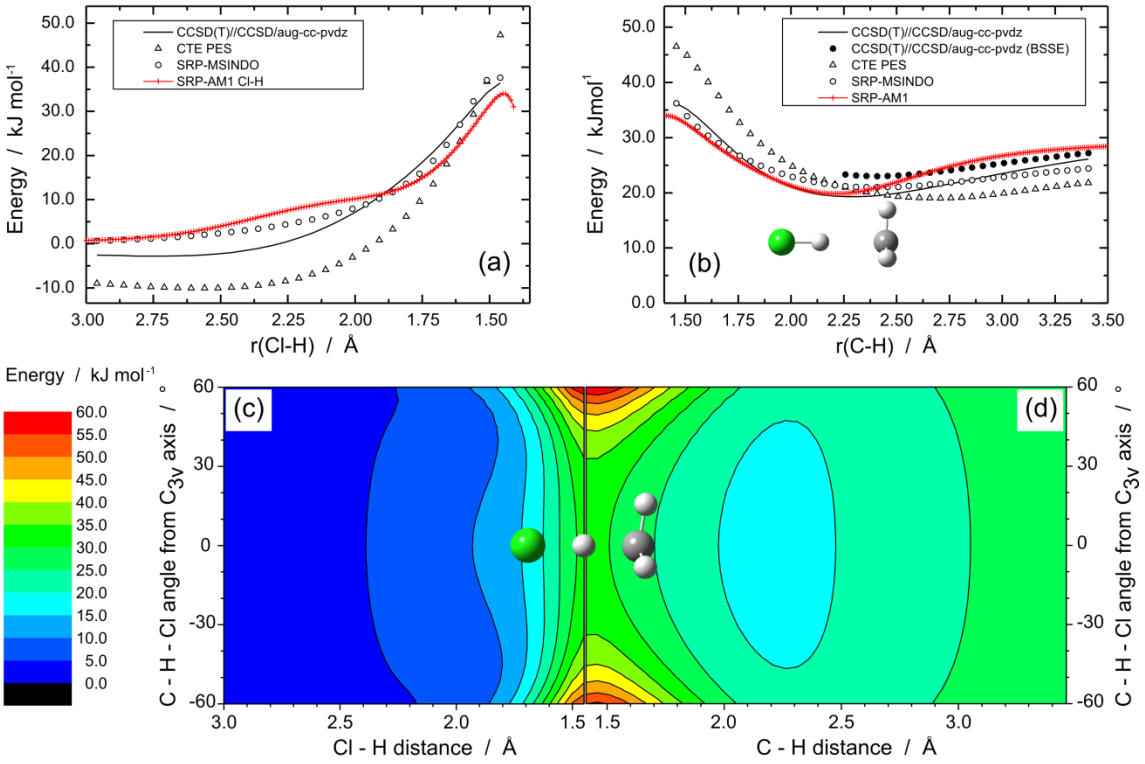

Figure 1. Relaxed energy scans along the $Cl+CH_4 \rightarrow HCl+CH_3$ IRC. (a) Scan is of the potential energy as the Cl–H distance is reduced from the separated reagents to the TS geometry. (b) Scan is of the potential energy as the C–H distance is extended from the TS towards products, also showing the location of the post-TS minimum. The insert shows the geometry of the complex associated with the potential energy minimum. The plots show the results of CCSD(T)/aug-cc-pvdz, SRP-MSINDO, CTE PES single-point calculations,[16] in comparison with our SRP-AM1 calculations. All results shown correspond to classical energies (i.e. they do not include ZPE correction), and zero energy is chosen to correspond to separated reagents. Panels (c) and (d) show the behaviour of the PES as the Cl-H-C angle is changed relative to the C_{3v} symmetry axis: (c) shows the coupling between the angle and the Cl-H distance [panel (a)], and (d) shows the coupling between the C-H distance [panel (b)] and the angle. Inset is an image of the structure of the TS.

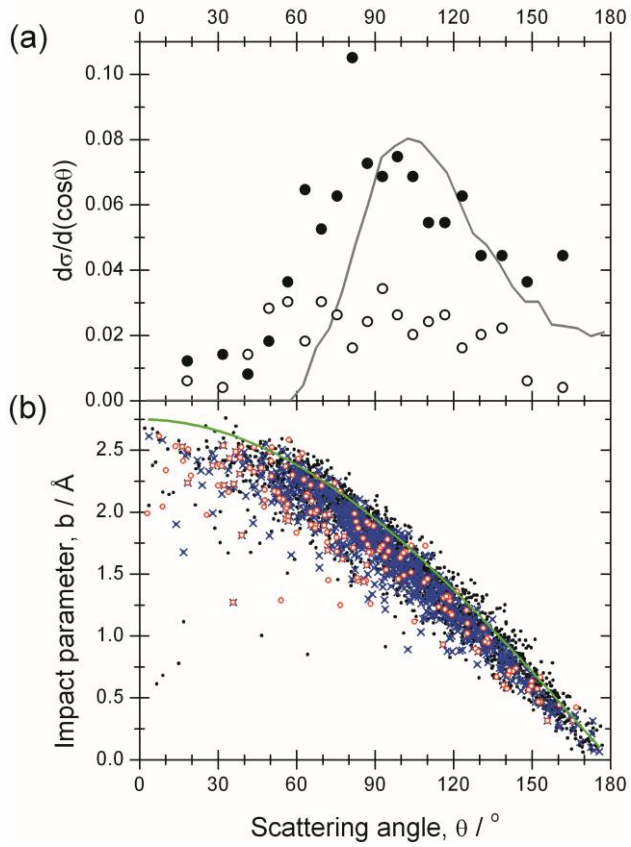

Figure 2. Panel (a), differential cross-section for the Cl+CH_4 reaction derived from QCT calculations. The plots compare the results after analysis of reactive trajectories that meet the criterion for radical product ZPE (see text for details) with the experimental results of Liu and co-workers (grey line) for the Cl+CH_4→CH_3(v=0)+HCl reaction pathway at a collision energy of 17.2 kJ mol^{-1}.[55] The QCT trajectories are separated into those producing ground state, CH_3(v=0), products (black circles), and those that have methyl radical umbrella bending mode excitation, CH_3(ν_2>0), open circles. No chattering trajectories are included in the computed DCSs. In the DCS plot, the scattering angles are divided into uniform cosθ bins of width 0.1. Panel (b) displays the correlation between scattering angle and impact parameter for all reactive trajectories (black dots), those that meet the criterion for radical product ZPE (blue diagonal crosses) and those that posses the signatures of chattering (red circles). The green line shows the prediction of the simple hard-sphere model,[56] with the hard-sphere radius, *d*, set to b_{max} = 2.75 Å.

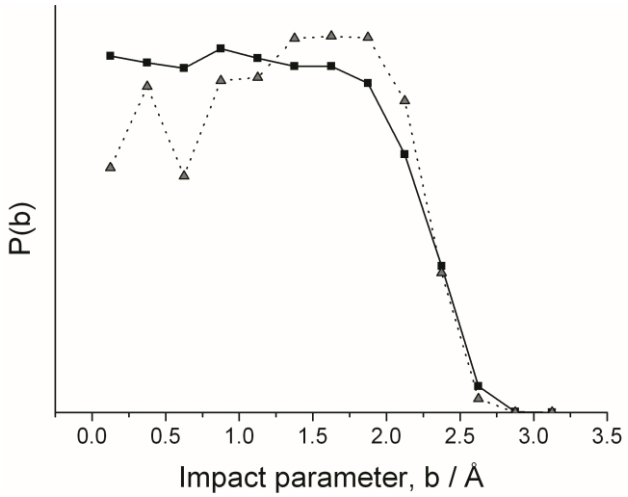

Figure 3. The opacity function, P(b), for the $Cl+CH_4 \rightarrow HCl+CH_3$ reaction for all reactive trajectories (black squares, solid lines), those that meet the criterion for radical product ZPE (dark grey triangles, dotted lines). The opacity function of the trajectories that meet the ZPE criterion has been multiplied by a factor of 4.0 to place it on the same scale at the function for all trajectories to allow ease of comparison of the profiles.

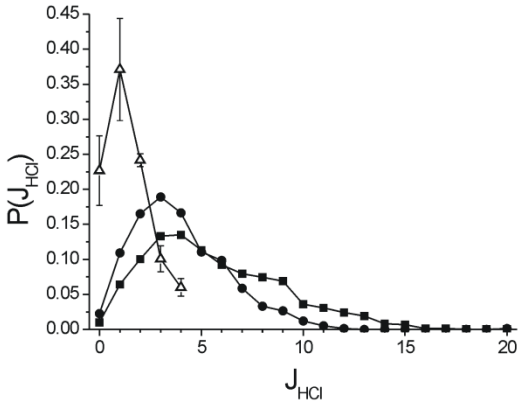

Figure 4. A comparison between calculated and experimental rotational distributions of the HCl product. The open black triangles are experimental data from ref. 45, at a mean collision energy of 15.4 kJ mol^{-1}. Black squares and circles indicate: all reactive trajectories, and those that meet the criterion for radical product ZPE, respectively.

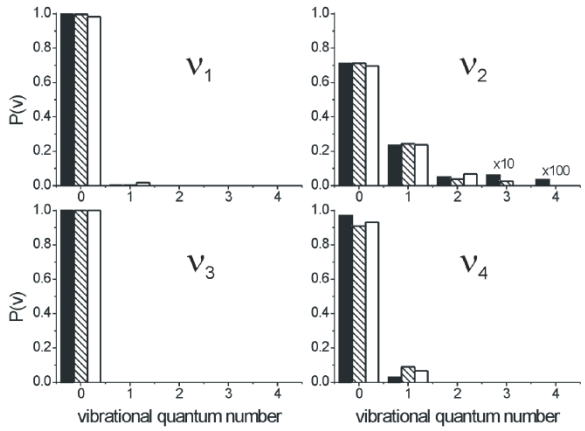

Figure 5. Calculated quantum-state-specific internal energy distributions of the CH_3 product of the $Cl+CH_4 \rightarrow HCl+CH_3$ reaction: the mode specific vibrational excitation of CH_3 in the symmetric stretch (v_1), umbrella bend (v_2), asymmetric stretch (v_3) and scissor bend (v_4) modes. Black bars represent all 2930 reactive trajectories, the 751 trajectories that meet the criterion for radical product ZPE are diagonal hashed and the white boxes represent 59 trajectories that have the signatures of chattering, all sets of trajectories have been normalised to unit area.